ECS Transactions, 19 (4) 15-26 (2009)
10.1149/1.3117388 ©The Electrochemical Society

Impact of Confinement of Semiconductor and Band Engineering on Future Device Performance

V. Sverdlov[a], O. Baumgartner[a], T. Windbacher[a], F. Schanovsky[b], S. Selberherr[a]

[a] Institute for Microelectronics
[b] C. Doppler Laboratory for TCAD at the Institute for Microelectronics
TU Wien, Gußhausstraße 27-29, 1040 Wien, Austria

A rigorous analysis of the subband structure in thin silicon films under stress is performed. Calculated subband effective masses are shown to depend on shear strain and thickness simultaneously. The effective masses and the subband splitting determine transport in silicon films. Decrease of the transport effective mass controlled by the shear strain component guarantees mobility enhancement even in ultra-thin silicon films. This increase of mobility and drive current combined with the improved channel control makes multi-gate MOSFETs based on thin films or silicon fins preeminent candidates for the 22nm technology node and beyond.

Introduction

The rapid increase in computational power and speed of integrated circuits is supported by the aggressive size reduction of semiconductor devices. Downscaling of MOSFETs as institutionalized by Moore's law is successfully continuing because of innovative changes in the technological processes and the introduction of new materials. The 32nm MOSFET process technology recently developed by Intel (1) involves new hafnium-based high-k dielectric/metal gates and represents a major change in the technological process since the invention of MOSFETs. Although alternative channel materials with a mobility higher than in Si were already investigated (2, 3), it is commonly believed that strained Si will be the main channel material even for MOSFETs beyond the 32nm technology node.
With scaling apparently approaching its fundamental limits, the semiconductor industry is facing critical challenges. New engineering solutions and innovative techniques are required to improve CMOS device performance. Strain-induced mobility enhancement is the most attractive solution to increase the device speed and will certainly take a key position among other technological changes for the next technology generations. In addition, new device architectures based on multi-gate structures with better electrostatic channel control and reduced short channel effects will be developed. A multi-gate MOSFET architecture is expected to be introduced for the 22nm technology node. Combined with a high-k dielectric/metal gate technology and strain engineering, a multi-gate MOSFET appears to be the ultimate device for high-speed operation with excellent channel control, reduced leakage currents, and low power budget.
Confining carriers within thin Si films reduces the channel dimension in transversal direction, which further improves gate channel control. The quantization energy in ultra-thin Si films may reach a hundred meV. The parabolic band approximation usually employed for subband structure calculations of confined electrons in Si inversion layers becomes insufficient in ultra-thin Si films. A recent study of subband energies and transport in (001) and (110) oriented thin Si films reveals that even non-parabolic

isotropic dispersion is not sufficient to describe experimental data, and a direction-dependent anisotropic non-parabolicity must be introduced (4).

A comprehensive analysis of transport in multi-gate MOSFETs under general stress conditions is required for understanding the enhancement of device performance. Besides the biaxial stress obtained in silicon films grown epitaxially on a SiGe substrate, modern techniques allow the generation of large uniaxial stress along the [110] channel. Stress in this direction induces significant shear lattice distortion. The influence of the shear distortion on subband structure and low-field mobility has not yet been carefully analyzed. The two-band **k·p** model (5-8) provides a general approach to compute the subband structure, in particular the dependence of the electron effective masses on shear strain. In case of a square potential well with infinite walls, which is a good approximation for the confining potential in ultra-thin Si films, the subband structure can be obtained analytically (9). This allows an analysis of subband energies, effective masses, non-parabolicity and the low-field mobility on film thickness for arbitrary stress conditions.

In the following we briefly review the main ideas behind the two-band **k·p** model for a valley in the conduction band of Si. Then we shortly analyze the unprimed subband structure in (001) ultra-thin Si films, obtaining analytical expressions for the effective masses and non-parabolicity parameter. With these parameters the non-parabolic subband approximations for the subband dispersions are constructed. The non-parabolic subband dispersions are embedded into a subband Monte Carlo code in order to enable the computation of the low-field mobility. Results of the mobility enhancement calculations are finally analyzed.

Conduction Band in Silicon

Two-band Hamiltonian

The subband structure in a confined system must be based on accurate bulk bands including strain, where several options are available. The conduction band dispersions computed with several methods in [100] and [110] directions are compared in Fig.1. The method based on non-local empirical pseudo-potentials from (10) is the most accurate one as compared to DFT band structure results obtained with VASP (11). The $sp^3d^5s^*$ tight-binding model with parameters from (12) does not reproduce the anisotropy of the conduction band correctly. In addition, an accurate calibration of the parameters of the $sp^3d^5s^*$ model to describe the modification of the conduction band in strained Si is still lacking.

The **k·p** theory is a well established method to describe the band structure analytically. As illustrated in Fig.1, the **k·p** method reproduces the band structure accurately at energies below 0.5eV, which is enough to describe the subband structure and transport properties of advanced MOSFETs. From symmetry consideration the two-band **k·p** Hamiltonian of a [001] valley in the vicinity of the *X* point of the Brillouin zone in Si must be in the form (6):

$$H = \left(\frac{\hbar^2 k_z^2}{2m_l} + \frac{\hbar^2 (k_x^2 + k_y^z)}{2m_t} \right) I + \left(D\varepsilon_{xy} - \frac{\hbar^2 k_x k_y}{M} \right) \sigma_z + \frac{h^2 k_z k_0}{m_l} \sigma_y \quad , \qquad [1]$$

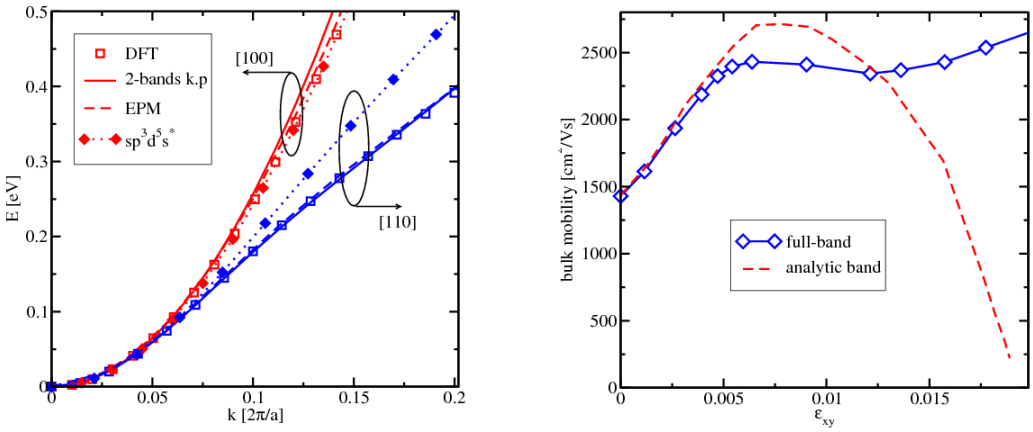

a. **b**.

Figure 1 **a**. Comparison of bulk dispersions close at the minimum of the [001] valleys of the conduction band in [100] and [110] directions. DFT (11) and EPM (7,10) results are similar, while the $sp^3d^5s^*$ tight-binding model (12) underestimates anisotropy significantly;
b. Bulk mobility computed by accounting for the full-band structure (symbols) and approximated with non-parabolic dispersion of six valleys (dashed line).

where $\sigma_{y,z}$ are the Pauli matrices, I is the 2×2 unity matrix, m_t and m_l are the transversal and the longitudinal effective masses, $k_0 = 0.15 \times 2\pi / a$ is the position of the valley minimum relative to the X point in unstrained Si, ε_{xy} denotes the shear strain component, $M^{-1} \approx m_t^{-1} - m_0^{-1}$, and D=14eV is the shear strain deformation potential (5-8). The two-band Hamiltonian results in the following dispersion relations (6):

$$E = \frac{\hbar^2 k_z^2}{2m_l} + \frac{\hbar^2 (k_x^2 + k_y^2)}{2m_t} \pm \sqrt{\left(\frac{\hbar^2 k_z k_0}{m_l}\right)^2 + \delta^2}\,, \qquad [2]$$

where the negative sign corresponds to the lowest conduction band,

$$\delta^2 = (D\varepsilon_{xy} - \hbar^2 k_x k_y / M)^2\,. \qquad [3]$$

All moments as well as energies in [2] are counted from the X-point of the Brillouin zone. The classical parabolic approximation is obtained from [2], when coupling between the two conduction bands described by the parameter δ is neglected. Coupling between the bands is small, when the wave vectors $|k_x|$, $|k_y| << k_0 (M/m_l)^{1/2}$ and shear strain $\varepsilon_{xy} = 0$. Due to band coupling the dispersion relations [2] become non-parabolic in strained Si, if the shear strain component is non-zero, and/or at higher energies. In order to check the accuracy of [2] we have carried out numerical band structure calculations with the empirical pseudo-potential method (EPM) with parameters from (7,10). Excellent agreement between the two-band **k·p** model [1] and the EPM results was found up to an energy of 0.5eV. Equation [2] is valid in a larger range of energies compared to a parabolic dispersion relation with isotropic non-parabolic correction and can be used to determine the subband structure in thin Si films.

Shear strain induced valley shift

It follows from [2] that the position of the conduction band minimum located at a distance k_0 from the X–point in unstrained silicon moves closer to the X–point for

nonzero shear strain. Introducing dimensionless strain $\eta = m_l D\varepsilon_{xy} / \hbar^2 k_0^2$, one finds for the position of the minimum (7,8):

$$k_{\min} / k_0 = \sqrt{1-\eta^2} \ . \qquad [4a]$$

At the same time, the minimum moves down in energy:

$$\Delta E_{\min} = -\eta^2 \Delta / 4 \ , \qquad |\eta| \le 1 , \qquad [4b]$$

where $\Delta = 2m_l / \hbar^2 k_0^2$ is the gap between the two conduction bands at the minimum k_0. For $|\eta| \ge 1$ the conduction band minimum stays exactly at the *X* point, resulting in the following energy dependence:

$$\Delta E_{\min} = -(2|\eta| - 1)\Delta / 4 \ , \qquad |\eta| \ge 1 . \qquad [4c]$$

Effective masses

Shear strain ε_{xy} modifies the effective masses of the [001] valleys. The transversal mass m_t acquires two different values along (+) and across (-) tensile stress direction (7,8):

$$m_t(\eta) / m_t = [1 \pm |\eta| m_t / M]^{-1}, \qquad |\eta| \le 1 ; \qquad [5a]$$

$$m_t(\eta) / m_t = [1 \pm m_t / M]^{-1}, \qquad |\eta| \ge 1 \ . \qquad [5b]$$

The longitudinal mass m_l is expressed as

$$m_l(\eta) / m_l = [1 \pm \eta^2]^{-1}, \qquad |\eta| \le 1 ; \qquad [6a]$$

$$m_l(\eta) / m_l = [1 \pm |\eta|^{-1}]^{-1}, \qquad |\eta| \ge 1 \ . \qquad [6b]$$

Non-parabolicity

From the two-band Hamiltonian the value of the non-parabolicity parameter is $\alpha_0 \approx 0.6\,\mathrm{eV}^{-1}$ (13). It is close to the phenomenological value $\alpha_0 = 0.5\,\mathrm{eV}^{-1}$ routinely used in calculations. Strain induced modification of the conduction band effective masses affects the nonparabolicity parameter α of the [001] valleys.

The expression for the density-of-states can be written in the form (14)

$$D(E) = \int \frac{dk_x dk_y}{(2\pi)^2} \delta(E - E_n(k_x, k_y)) = \frac{\sqrt{m_-(\eta) m_+(\eta)}}{(2\pi)^2} \int\limits_{E=const} d\varphi \frac{1}{2} \frac{\partial \zeta^2(E,\varphi)}{\partial E} , \qquad [7]$$

where $\zeta^2(E,\varphi) = k_-^2 / m_t^-(\eta) + k_+^2 / m_t^+(\eta)$ is determined by the expression:

$$E = \frac{\zeta^2}{2} - \frac{\hbar^2 m_l}{8M^2 k_0^2 |1 - q_n^2|} \left(m_- \cos^2\varphi - m_+ \sin^2\varphi\right)^2 \zeta^4 . \qquad [8]$$

Substituting [8] into [7] and assuming the energy *E* close to the valley minimum so that $\alpha E << 1$, we obtain the following expression for the non-parabolicity parameter ratio:

$$\alpha = \alpha_0 \frac{1 + 2\left(m_t \eta / M\right)^2}{\left(1 - \left(m_t \eta / M\right)^2\right)^2} . \qquad [9]$$

The relative increase of α resulting in an increased density of states and scattering are responsible for a weaker mobility enhancement (Fig.1b) as compared to the mobility obtained with strain-independent α_0. However, for a stress larger than 3 GPa ($\eta \ge 0.5$) the energy difference from the minimum to the value at the *X* point becomes smaller than *kT*, and a full-band description is required for accurate mobility calculations (15).

Subbands in Ultra-Thin Silicon Films

Dispersion equations

For [001] silicon films the confinement potential gives an additional contribution $U(z)I$ to the Hamiltonian [1]. In the effective mass approximation described by [1] with the coefficient in front of σ_x set to zero, the confining potential $U(z)$ is known to quantize the six equivalent valleys of the conduction band of bulk silicon into the four-fold degenerate primed and the two-fold degenerate unprimed subband ladder (16). In ultra-thin films the unprimed ladder is predominantly occupied. In order to analyze the subbands, we approximate the confining potential of an ultra-thin silicon film by a square well potential with infinite potential walls. Generalization to include a self-consistent potential is straightforward though numerically involved (17).

Because of the two-band Hamiltonian, the wave function Ψ is a spinor with the two components |0> and |1>. For a wave function with space dependence in the form $\exp(ik_z z)$ the coefficients A_0 and A_1 of the spinor components are related via the equation $H\Psi = E(k_z)\Psi$. For a particular energy E there exist four solutions k_i (i=1,…,4) for k_z of the dispersion relation [2], so the spatial dependence of a spinor component is in the form $\sum_{i=1}^{4} A_\alpha^i \exp(ik_i z)$. The four coefficients are determined by the boundary conditions that both spinor components are zero at the two film interfaces. This leads to the following dispersion equations:

$$\tan\left(k_1 \frac{k_0 t}{2}\right) = \frac{k_2}{\sqrt{k_2^2+\eta^2}\pm\eta} \frac{\sqrt{k_1^2+\eta^2}\pm\eta}{k_1} \tan\left(k_2 \frac{k_0 t}{2}\right) \quad , \qquad [8]$$

where $\eta = m_l |\delta| /(\hbar k_0)^2$. If the value of

$$k_2 = \sqrt{k_1^2 + 4 - 4\sqrt{k_1^2+\eta^2}} \qquad [9]$$

becomes imaginary at high η values, the trigonometric functions in [8] are replaced by the hyperbolic ones. Special care must be taken to choose a correct branch of $\sqrt{k_2^2+\eta^2}$ in [9]: the sign of $\sqrt{k_2^2+\eta^2}$ must be alternated after the argument becomes zero. Introducing $y_n = (k_1 - k_2)/2$, [8] can be written in the form (18):

$$\sin(y_n k_0 t) = \pm \frac{\eta y_n \sin\left(\frac{1-\eta^2-y_n^2}{1-y_n^2} k_0 t\right)}{\sqrt{(1-y_n^2)(1-\eta^2-y_n^2)}} \quad . \qquad [10]$$

Subband structure in thick films

We solve [10] by perturbation techniques. For small η and thick films the right-hand side in [10] can be ignored. The subband relations are found from the condition

$$y_n = \pi n /(k_0 t) \, . \qquad [11]$$

This results in the following approximate dispersion relation for unprimed subbands (16):

$$E_n(k_x, k_y) = E_n^0(k_x, k_y) - \Delta\eta^2 /[4\,|1-q_n^2\,|] \, , \qquad [12]$$

where $q_n = (\pi n)/(tk_0)$ and E_n^0 is the subband dispersion relation for parabolic bands:

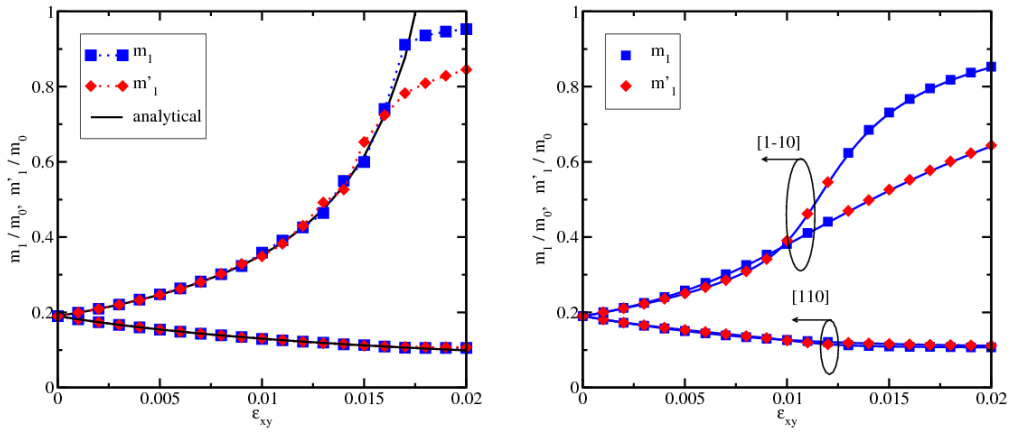

a. **b**.

Figure 2 Effective masses of the two ground subbands. Symbols are obtained by numerical solution of the two-band Hamiltonian [1]:
a. t=10.86nm; solid lines are according to [16];
b. t=5.43nm; solid lines are obtained by numerically differentiating subband dispersions obtained from [8].

$$E_n^0(k_x,k_y)=\frac{\hbar^2\pi^2n^2}{2m_lt^2}+\frac{\hbar^2(k_x^2+k_y^2)}{2m_t}-\frac{\hbar^2k_0^2}{2m_l}.$$

[12] is valid when

$$\left(1-q_n^2\right)^2 >> \delta^2 m_l^2/\hbar^4k_0^4. \qquad [13]$$

Equation [12] describes the subband quantization energy correction due to strain with respect to the valley minimum

$$\Delta E_n(\eta)=-\frac{\hbar^2\pi^2n^2}{2m_lt^2}\frac{\eta^2}{|1-q_n^2|}, \qquad [14]$$

which is obtained after taking into account the strain-induced valley minimum energy shift $\Delta E_{\min}$. [14] can be absorbed into the quantization energy $\frac{\hbar^2\pi^2n^2}{2m_lt^2}$ by introducing the longitudinal mass m_l depending on strain η and thickness t:

$$m_l(\eta,q_n)=\frac{m_l}{1-\eta^2/|1-q_n^2|}. \qquad [15]$$

[12] also describes dependencies of the transversal masses on strain η, the film thickness t, and subband number n:

$$m_t^{\mp}(\eta,q_n)=m_t\left(1\pm\eta\frac{m_t}{M}\frac{1}{|1-q_n^2|}\right)^{-1}. \qquad [16]$$

Here m_t^- is the effective mass along the direction [110] of tensile stress. In films the effective mass depends not only on strain but also on film thickness. We compare [16] (lines) with the results of the numerical solution of the two-band **k·p** model Hamiltonian (symbols) in a film with the thickness t=10nm for the ground (n=1) (shown in Fig.2a) and the second (n=2) subbands and find a good agreement. With the film thickness decreased and strain increased a substantial discrepancy between [16] and a numerical

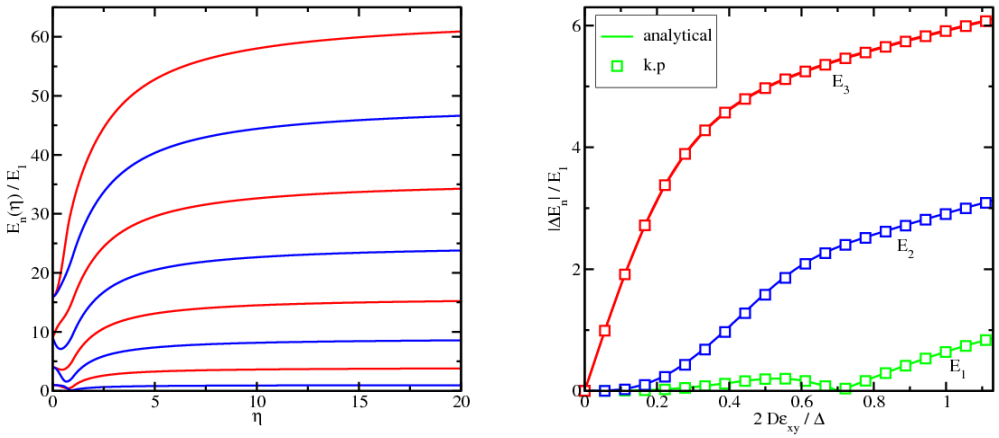

a. **b**.

Figure 3 **a**. Normalized positions of the subband minima with respect to the strain-dependent conduction band minimum as function of dimensionless shear strain for a film of the thickness t=5.43nm.
b. Strain-dependent splitting between the minima of the unprimed subbands with the same n.

solution appears as shown in Fig.2b. This discrepancy is caused by the growing value of the right-hand side in [10] which cannot be ignored.

Splitting of unprimed subbands

Substituting [11] into the right-hand side of [10] and solving [10] for small strain η one obtains the following dispersion relation for the unprimed subbands n:

$$E_n^{\pm} = \frac{\hbar^2}{2m_l}\left(\frac{\pi n}{t}\right)^2 + \hbar^2\frac{k_x^2+k_y^2}{2m_t} \pm \left(\frac{\pi n}{k_0 t}\right)^2 \frac{\left| D\varepsilon_{xy} - \dfrac{\hbar^2 k_x k_y}{M}\right|}{k_0 t\left|1-(\pi n/k_0 t)^2\right|}\sin(k_o t)\ . \qquad [17]$$

It follows that the subband degeneracy is preserved only, when shear strain is zero and either k_x=0 or k_y=0. [17] demonstrates that the unprimed subbands are *not equivalent*. We first analyze the splitting in energy between the two unprimed subbands with the same n, which is usually called the valley splitting (16). According to [17], shear strain induces a valley splitting linear in strain, for small shear strain values (18):

$$\Delta E_n = 2\left(\frac{\pi n}{k_0 t}\right)^2 \frac{D\varepsilon_{xy}}{k_0 t\left|1-(\pi n/k_0 t)^2\right|}\sin(k_o t)\ . \qquad [18]$$

The valley splitting is inversely proportional to $(k_0 t)^3$ and oscillates with the film thickness, in agreement with earlier work (16,19).
To find the valley splitting at higher strain values, [10] must be solved numerically. Results shown in Fig.3 demonstrate that valley splitting can be effectively controlled by adjusting the shear strain and modifying the effective thickness t of the electron system. It is interesting to note that for extremely high strain values the dispersion of the lowest conduction band becomes parabolic again, and the quantization levels in a square well potential are therefore recovered in this limit. Although the value of strain in this limit is unrealistic, this result will be used to analyze dispersion relations for the primed subbands.

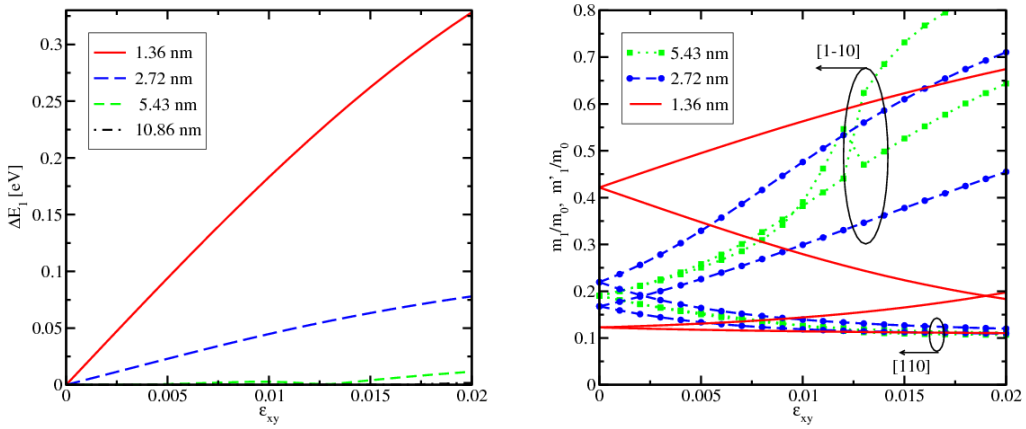

a. **b**.

Figure 4 **a**. Shear strain induced splitting of the ground subbands for several film thicknesses. In ultra-thin films splitting is larger than *kT* already for moderate stress. **b**. Effective masses of the two ground subbands. In ultra-thin films effective masses of the two ground subbands are different even without stress.

Uniaxial stress along [110] channel direction, which induces shear strain, is already used by industry to enhance the performance of modern MOSFETs. Therefore, its application to control valley splitting does not require expensive technological modifications. A possibility to introduce valley splitting larger than the Zeeman spin splitting makes Si promising for future spintronic applications (20).

As seen from Fig.4a, the valley splitting in ultra-thin Si films can be quite large already for reasonable stress values. In this case the higher subband becomes depopulated, prompting for mobility enhancement in (001) ultra-thin films strained along [110] direction.

Effective masses of unprimed subbands

Dispersion [17] predicts different effective masses in [110] direction for the unprimed subbands with the same *n* even without strain:

$$m_{(1,2)} = \left(\frac{1}{m_t} \pm \frac{1}{M} \left(\frac{\pi n}{k_0 t} \right)^2 \frac{\sin(k_o t)}{k_0 t \,|\, 1 - (\pi n / k_0 t)^2 \,|} \right)^{-1} \qquad [19]$$

Numerically found values of the masses for the two ground subbands are shown in Fig.4b. Contour plots of the subband dispersions for the two ground subbands are shown in Fig.5. It is to note, that the subband dispersions are not equivalent. This has a profound effect on the valley splitting. Without shear strain the Landau levels in the external [001] magnetic field *B* are determined using the Bohr-Sommerfeld quantization conditions:

$$E_m^{(1,2)} = \hbar \omega_c \left(m + \frac{1}{2} \right) \frac{\pi}{4 \arctan\left(\sqrt{m_{(1,2)} / m_{(2,1)}} \right)}, \qquad [20]$$

where $\omega_c = \frac{eB}{\sqrt{m_1 m_2}\, c}$ is the cyclotron frequency. Therefore, the magnetic field induces a valley splitting linear in the field strength *B*, in agreement with recent experimental results (20).

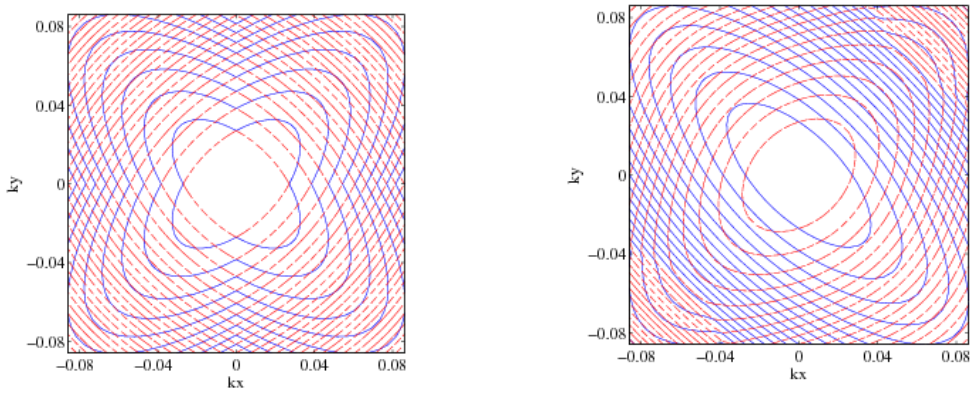

a. **b**.

Figure 5 Dispersions of the two ground subbands for a film thickness of 1.36nm:
a. Without strain the subbands are degenerate at the minimum. The lower subband dispersion is described by the unification of the two ellipses with different masses [19], while the second subband is described by their intersection. The difference in quasi-classical orbits of the motion in the magnetic field is responsible for the subband splitting [20] in orthogonal magnetic field.
b. Shear strain of 1% removes the degeneracy between the minima of the ground subbands shown in Fig.4a. The subband dispersions are now characterized by the corresponding effective masses in [110] and [1-10] directions (Fig.4b).

A large value of the valley splitting observed by measuring conductance through a point contact can also be attributed to the difference in the subband dispersions, in particular, to the effective mass difference [19]. Indeed, confining the electron system laterally in [1-10] direction by the potential, the following dispersion relation of propagating modes within the point contact is obtained:

$$E_p^{(1,2)} = \frac{k^2 k_x'^2}{2m_{(2,1)}} + \hbar\omega_{(1,2)}\left(p + \frac{1}{2}\right) + V_b \,. \qquad [21]$$

Here $\omega^2_{(1,2)} = \kappa / m_{(1,2)}$ and V_b is a gate voltage dependent shift of the conduction band in the point contact (21). The energy minima of the two propagating modes with the same p are separated by $\Delta E_p = \hbar\,|\,\omega_1 - \omega_2\,|$ and they are resolved in the conductance of a point contact as two distinct steps. The difference in the effective masses [17] and, correspondingly, the valley splitting can be greatly enhanced by reducing the effective thickness t of the film.

Effective mass of primed subband

Shear strain in [110] direction does not affect the primed valleys along [100] and [010] direction, except for a small shift of the minimum (22). However, recent calculations of the primed subbands based on the density functional theory (23) and the "linear combination of bulk bands" method obtained with the empirical pseudo-potential calculations (24) reveal the dependence of the transport effective masses on silicon film thickness t. Here we briefly analyze the effective mass of the primed subbands based on the two-band Hamiltonian [1]. Let us assume the quantization direction along the X-axis. By formally replacing k_0/m_l with k_y/M and k_x k_y/M with k_z k_0/m_l in [1] one finds the

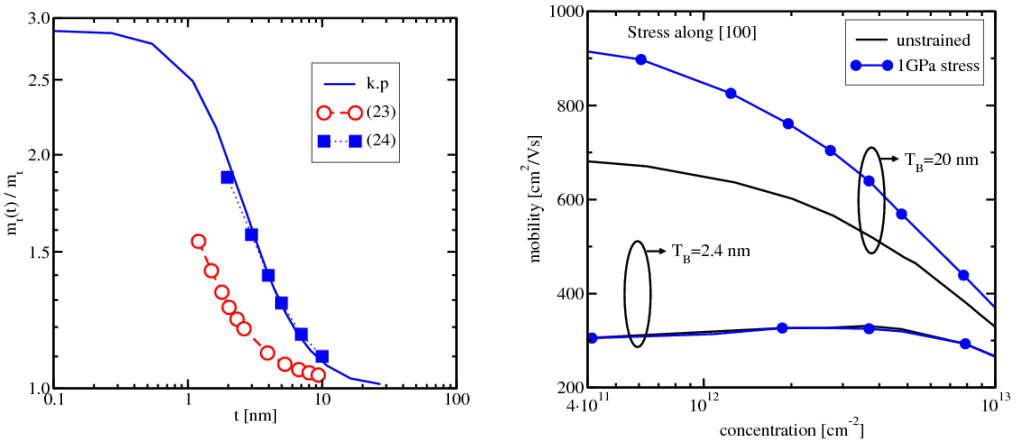

a. **b**.

Figure 6 **a**. The thickness dependence of the effective mass of the lowest primed subbands computed with the two-band **k·p** model (solid line) is in excellent agreement with the full-band calculations (24) (filled symbols). Open symbols show calculations from (23).
b. The mobility enhancement in [100] direction due to [100] tensile stress of 1GPa is due to de-population of the primed subbands with an unfavourable effective mass in transport direction. In ultra-thin films, where the primed subbands are already de-populated ,mobility remains unchanged.

dispersion and the effective masses in the primed subbands, where results of calculations are shown in Fig.6a. The two-band **k·p** results are in excellent agreement with the "linear combination of the bulk bands" method with a potential barrier of 3eV at the film interface (24) and they are also consistent with the DFT calculations (23).

Mobility Enhancement due to Uniaxial Stress

A multi-subband Monte Carlo method designed for small signal analysis (25) was used to evaluate the mobility in MOSFETs with a thin Si film. The method is based on the solution of the linearized multi-subband Boltzmann equation, which is exact in the limit of vanishing driving fields. A particular advantage of the method is that it includes degeneracy effects due to the Pauli exclusion principle. Degeneracy effects are important for mobility calculations in ultra-thin films, especially at high carrier concentrations. The multi-subband method uses the subband wave functions and subband energies. They can be found by solving the Schrödinger equation and the Poisson equation self-consistently for each value of the gate voltage (17). The wave functions are then employed to evaluate scattering rates. Scattering with phonons and surface roughness is included. The surface roughness at the two thin film interfaces is assumed to be equal and uncorrelated. The parameters of the Gaussian surface roughness correlation function were calibrated to reproduce the universal mobility curve of Takagi (26) in the inversion layer. The same parameters are then used for mobility calculations in thin film MOSFETs.
Fig.6b displays the mobility in (001) silicon films for two film thicknesses under a tensile uniaxial stress of 1GPa in [100] direction. The stress shifts up and de-populates the two [100] primed valleys with unfavorable mass m_l in the transport direction providing the mobility enhancement in the stress direction for a 20nm film. In [010] transport direction the [100] primed valleys have a smaller transversal mass. Therefore, the de-population of the [100] primed subbands due to [100] tensile stress has a detrimental effect on the

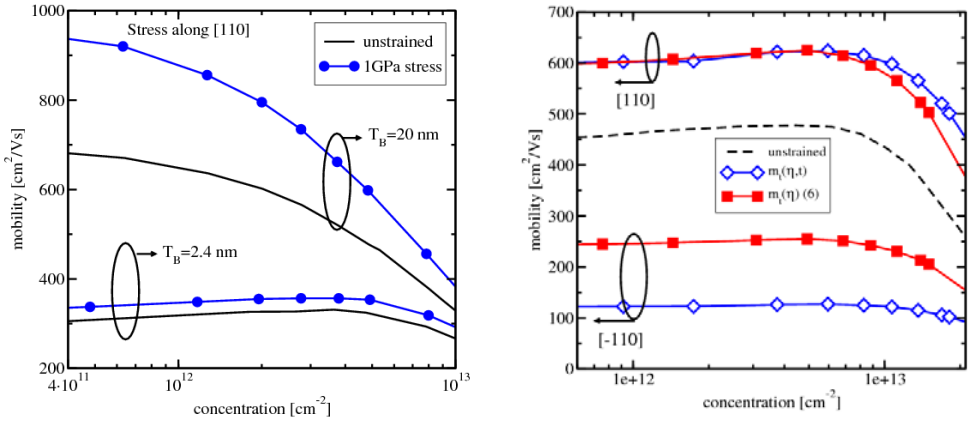

a. **b**.

Figure 7 **a**. The mobility enhancement due to tensile stress of 1GPa in [110] transport direction due to transport mass decrease is preserved even in ultra-thin films.
b. Mobility in a 3 nm thick film as a function of electron concentration calculated for 0.5% tensile shear strain in [110] direction, with bulk effective masses [6] (filled symbols) and with strain- and thickness-dependent masses (Fig.4b) (open symbols). The increase of the density-of-states effective mass with strain enhances scattering which alters the mobility enhancement in [110] direction.

mobility in [010] direction. In ultra-thin films the primed subbands are nearly de-populated already without stress due to the large separation in energy between primed and unprimed subbands in a silicon film with a thickness of 2.4nm. Therefore, additional shifting up in energy of the [100] valleys does not have any effect on the mobility in ultra-thin films (Fig.6b).
Apart from shifting primed subbands with unfavorable transport masses in the (001) plane up in energy and de-populating them, tensile stress in [110] direction generates a shear component which modifies the transport effective masses of unprimed subbands (Fig.4b). The decrease of the effective masses in [110] direction induced by shear strain becomes more pronounced with the film thickness reduced guaranteeing the mobility enhancement even in ultra-thin films, as demonstrated in Fig.7a. However, the density-of-state effective mass $m^* = \sqrt{m_t^+ m_t^-}$ in unprimed subbands increases with shear strain. This results in higher scattering rates which deteriorate the benefits of the thickness-enhanced transport mass decrease at higher stress values, as displayed in Fig.7b. However, the mobility enhancement remains substantial.

Conclusion

A rigorous analysis of the subband structure in thin silicon films is performed. The thickness dependence of the effective mass of primed subbands calculated within the two-band **k·p** model is in agreement with the earlier full-band calculations. It is demonstrated that within the two-band **k·p** model the unprimed subbands with the same quantum number *n* are not equivalent. A large splitting between the unprimed valleys of ultra-thin films can be introduced by a shear strain component. Calculated subband effective masses are shown to depend on shear strain and thickness simultaneously. Interestingly, the effective masses of the two unprimed valleys are different in ultra-thin silicon films even without strain. This results in a linear dependence of the subband

splitting on the magnetic field strength and leads to large subband splitting in a laterally confined electron system in a point contact.

The mobility enhancement in strained MOSFETs with ultra-thin silicon films is investigated by a subband Monte Carlo method. The method based on the solution of the linearized Boltzmann equation includes the carrier degeneracy exactly. Transport in thin films is determined by subband structure, in particular by the effective masses. The decrease of the transport effective mass induced by the shear strain component is the reason for the mobility enhancement even in ultra-thin silicon films. This mobility and drive current increase combined with the improved channel control makes multi-gate MOSFETs based on thin films or silicon fins preeminent candidates for the 22nm technology node and beyond.

Acknowledgments

This work was supported in part by the Austrian Science Fund FWF, project P19997-N14, and by funds from FWF, project I79-N16, CNR, EPSRC and the EC Sixth Framework Programme, under Contract N. ERAS-CT-2003-980409 as part of the European Science Foundation EUROCORES Programme FoNE.

References

1. S.Natarjan, M.Armstrong, H.Bost, *et al*., *IEDM* 2008, pp.941-943.
2. M.K.Hudati, G.Dewey, S.Datta, *et al*., *IEDM* 2007, pp.625-628.
3. R.Chau, *ISDRS* 2007, p.3.
4. K.Uchida, A.Kinoshita, M.Saitoh, *IEDM* 2006, pp.1019-1021.
5. J.C.Hensel, H.Hasegawa, and M.Nakayama, *Phys.Rev*. **138**, A225-A238 (1965).
6. G.L.Bir, G.E.Pikus, Symmetry and Strain-Induced Effects in Semiconductors, J.Willey & Sons, NY, 1974.
7. E.Ungersboeck, S.Dhar, G.Karlowatz, *et al.*, *IEEE T-ED* **54**, 2183-2190 (2007).
8. V.Sverdlov, E.Ungersboeck, H.Kosina, S.Selberherr, *ESSDERC* 2007, pp.386-9.
9. V.Sverdlov, G.Karlowatz, S.Dhar, *et al*., *Sol.State Electron.* **52**, 1563-1568 (2008).
10. M.Rieger and P.Vogl, *Phys.Rev. B* **48**, 14275-14287 (1993).
11. VASP (Vienna Ab-initio Simulation Program) G.Kresse and J. Hafner, Phys.Rev. B 47, 558 (1993); ibid. B 49, 14251 (1994); G.Kresse and J. Fertmueller, Phys.Rev. B 54, 11169 (1996); Comput.Mat.Sci. 6, 15 (1996).
12. T.B.Boykin, G.Klimeck, and F.Oyafuso, *Phys.Rev.B* **69**, 115201-1—10 (2004).
13. C.Jacoboni, L.Reggiani, *Rev.Mod.Phys.* **55**, 645-705 (1983).
14. M.V.Fischetti, S.E.Laux, *Journal of Applied Physics* **80**, 2234-2252 (1996).
15. V.Sverdlov, G.Karlowatz, E.Ungersboeck, H.Kosina, *SISPAD* 2007, pp.329-332.
16. T.Ando, A.B.Fowler, F.Stern, *Rev.Mod.Phys.* **54**, 437-672 (1982).
17. O.Baumgartner, M.Karner, V.Sverdlov, H.Kosina, *EUROSOI* 2009, pp.57-58.
18. V.Sverdlov and S.Selberherr, *Sol.State Electron.* **52**, 1861-1866 (2008).
19. M.Friessen, S.Chutia, C.Tahan, *et al.*, *Phys.Rev.B* **75**, 115318-1—12 (2007).
20. S.Goswami, K.A.Slinker, M.Friesen, *et al.*, *Nature Physics* **3**, 41-45 (2007).
21. B.J.van Wees, H.van Houten, C.Beenakker, *Phys.Rev.Lett.*, **60**, 848-850 (1988).
22. D.Rideau, M.Feraille, M.Michaillat, *et al.*, *Sol.State Electron.* 2009, (online).
23. A.Martinez, K.Kalna, P.V.Sushko, *et al.*, *IEEE T-Nano* 2009 (online).
24. J.van der Steer, D.Esseni, P.Palestri, *et al.*, *IEEE T-ED* **54**, 1843-1851 (2007).
25. V.Sverdlov, E.Ungersboeck, H.Kosina, *et al.*,*Sol.StateElectron*.**51**, 299-305 (2007).
26. S.-I.Takagi, A.Toriumi, M.Iwase, H.Tango, *IEEE T-ED* **41**, 2357-2362 (1994).